www.czasopisma.pan.pl PAN www.journals.pan.pl

ARCHIVES of FOUNDRY ENGINEERING

ISSN (2299-2944)

10.24425/afe.2025.155367

Published quarterly as the organ of the Foundry Commission of the Polish Academy of Sciences

Corrosion Studies of Selective Laser Melting Printed AlSi10Mg Parts

Nagareddy Gadlegaonkar [a], Premendra J. Bansod [a], Avinash L [b, **], Krishnakant Bhole [c], Manjunath Patel G C [d, *], Nagaraja C. Reddy [e], Srilatha Rao [f]

[a] Department of Mechanical Engineering, G.H. Raisoni College of Engineering & Management, Wagholi, Affiliated to Savitribai Phule Pune University, Pune, Maharashtra, India

[b] Nitte (Deemed to be University), Nitte Meenakshi Institute of Technology (NMIT), Department of Mechanical Engineering, Bengaluru, 560064, India

[c] School of Design, Presidency University, Bangalore - 560064, India

[d] Department of Mechanical Engineering, Sahyadri College of Engineering & Management, Mangaluru, Visvesvaraya Technological University, Belagavi 590018, Karnataka, India

[e] Department of Mechanical Engineering, Bangalore Institute of Technology, Bengaluru - 560004, Karnataka, India

[f] Nitte (Deemed to be University), Nitte Meenakshi Institute of Technology (NMIT), Department of Chemistry, Bengaluru, 560064, India

*, ** Corresponding authors: E-mail address: manju09mpm05@gmail.com; & avinash.l@nmit.ac.in

Received 29.12.2024; accepted in revised form 02.04.2025; available online 26.08.2025

Abstract

$AlSi_{10}Mg$ alloy is widely used in marine, nuclear, petrochemicals, and food processing application parts operated in corrosive environments. A selective laser melting technique is used to print the $AlSi_{10}Mg$ parts. The printed specimen quality is influenced by laser power (LP), scan speed (SS), and hatch distance (HD). Taguchi L_9 orthogonal array is used for experimental planning, analysis, and optimising printed parts' corrosion resistance. LP is the most dominating factor, followed by hatch distance and scan speed on the corrosion current (corrosion resistance of sample). Taguchi method determined optimal conditions (LP: 270 W; SS: 1000 mm/s; HD: 0.10 mm) improve the corrosion resistance by 16.1%. The microstructure under optimal conditions exhibits minimal corrosion and oxidation on the sample surface compared to sub-optimal conditions examined with scanning electron micrographs. Any novice user can use the results of the optimal conditions for reduced corrosion current in the printed parts.

Keywords: AlSi10Mg, SLM Process, Taguchi analysis, Corrosion, SEM

1. Introduction

Aluminium alloys are widely accepted due to their excellent properties (mechanical strength, chemical stability, resistance to creep, and aqueous solutions) at elevated temperatures [1, 2]. The aforementioned properties ensure aluminium alloys are treated as advanced engineering materials and have proven their potential applications in aerospace, marine, engine parts, turbine, petrochemical, and nuclear reactors [3-5]. Furthermore, marine and plants (parts of nuclear, petrochemical, and food processing industries) find stringent applications in aggressive environments [6]. Machining aluminium alloys viz., grinding operation to meet the design requirements of the parts of applications above, requires better mechanical properties in addition to resistance to corrosion [7, 8]. The surface texture of machined components also

influences the corrosion resistance [9]. The corrosion behaviour of samples varies concerning different processes and their parameters [10, 11]. Therefore, studying different processes and optimizing influencing parametric combinations to improve corrosion resistance requires worldwide research attention.

Additive manufacturing technologies employ layer-by-layer deposition to build parts better than conventional processing routes, offering better dimensional accuracy for fabricating complex geometry profiles at reduced tooling cost [12, 13]. Seven major classifications of AM techniques were developed in the past two decades [14]. Selective Laser Melting (SLM) processing route employs the desirable features of powder metallurgy and casting methods [15]. The key takeaways of the SLM process are [16]: a) the ability to build parts from simple profile parts to complex geometries, b) material microstructure evolution from single homogeneous to multi-material gradient. SLM process transforms powders into solid parts subjected to cyclic heating and cooling, resulting in non-uniform microstructure and plasticity characteristics [17, 18]. This could induce residual stresses in-built parts and cause deformation and cracks [19]. During their service life, residual stresses undergo fatigue crack, which causes brittle fractures and induces stress corrosion [20]. Significant grain refinement in microstructure leads to better tensile strength, hardness, and corrosion resistance [21, 22] and strongly correlates with the SLM process variables [23, 24]. Notably, the selective laser melting variables depend largely on mechanical and tribological properties [22]. Important to note that the selective laser melting variables depend largely on mechanical and tribological properties [23, 24]. Therefore, there is significant scope to study the SLM variable's influence on the corrosion resistance of build parts.

In recent years, attempts have been made with selective laser melting techniques by distinguished researchers worldwide to enhance the quality of the parts by conducting experimental, analytical, and numerical tools and methods [25-29]. However, the analytical model and numerical finite elemental (FE) models use many assumptions while examining the thermal behaviour during building Alsi10Mg parts [29]. The FE method over-predicted the melt pool width at higher heat input power, probably due to assumptions in developing the model [25]. The assumptions used to obtain the potential solutions led to less realistic and impractical obtaining global solutions. The experimental approach is applied to investigate the effect of variables (factors of laser and scanning, material properties, powder bed characteristics, and so on) on outputs (melt pool size, density, surface and structural integrity, overlap rate, residual stress, mechanical properties and so on) of the build parts [30-32]. Many process variables influence the quality of the parts, and studying all variables at once, viz., trial-and-error experimental approach, is impractical (i.e., time-consuming, material waste, costlier, and so on). The statistical Taguchi method is applied to plan minimum experiments and optimize the process outcomes [24, 33-35]. Laser power, scan rate, hatch spacing, scan pattern, and build orientation are the major SLM parameters investigated and optimized for the outputs (hardness, density, surface roughness, dynamic stress, and so on). The above literature review confirmed that significant research efforts were made to study the process variables and analyze their effects that could optimize the mechanical and physical properties. AlSi10Mg alloys are widely used in marine applications, and corrosion studies are neglected in most research works.

Aluminium alloys find major applications in marine and other (parts of nuclear, petrochemical, and food processing industries) parts subjected to aggressive environments. These applications require materials and parts that provide greater corrosion resistance. SLM parts have proven to have greater potential to offer better mechanical and physical properties. The present work aims at a systematic and cost-effective approach to optimize for minimum corrosion rate in AlSi10Mg parts. The selection of appropriate levels for a process variable is challenging due to the large number of influencing variables and the requirements to conduct large experimental trials in SLM. Therefore, the Taguchi method is used to plan experiments and draw inferences based on collected experimental data by applying analysis of variance. The contribution of each variable to the corrosion resistance of AlSi10Mg parts was studied. The optimal parametric conditions responsible for minimizing the corrosion rate in building parts were determined and validated by conducting experiments.

2. Materials and Methods

This section discussed the materials used, the experimental matrix designed, the analysis conducted, the preparation of corrosion samples and examination, and the determining optimal conditions.

2.1. Materials and Process Variables

AlSi10Mg metal powders with an average size of < 35 µm were used to build the cube samples. The Laser spot size used in the current work is 70 µm and Argon (Ar) gas is used as shielding atmosphere to prevent oxidation and contamination during melting. Figure 1 depict a schematic of the SLM process. Metal powder is supplied from the powder supply compartment and distributed uniformly over the build assembly area by the powder roller. The laser nozzle smelts the powder by fusing it into the required geometry for that layer. The build stage travels down after every deposit is completed, and the procedure repeats till a fully deposited model is formed. In the SLM process, many variables (such as laser power, scan rates, atmospheric control, gas flow, bed type, scan length, scan spacing, layer thickness and machine type) influence the material properties and, in turn, impact the printing quality [36, 37]. Laser power and scan speed impact directly on the heat input, affecting the viscosity, melt temperature and thermal conductivity [38]. Atmospheric control and gas flow monitor the oxidation and ensure a stable environment, preserving chemical composition and surface tension [39]. The bed temperature and layer thickness affect the cooling rates (or thermal gradients), affecting the particle bonding and microstructure [40]. The component densification is influenced by scan patterns, spacing, and machine-specific parameters affecting the particle distribution, shape and absorptivity. The LP, SS, layer thickness and hatch distance were the major parameters influencing the properties of the printed parts [41-43]. The relative interdependencies among the process parameters and desired response optimization made the authors

select different operating conditions for the same AlSi10Mg material [36, 44]. Therefore, pilot experimental trials were conducted to decide the operating variables and consulting literature [23, 44, 36]. The levels of each parameter were fixed. Table 1 details the process parameters and operating levels used for experimentation.

Table 1.
Input variables of SLM process

Levels	Variables		
	Laser power, W	Scan speed, mm/s	Hatch distance, mm
Low	240	600	0.08
Medium	270	800	0.10
High	300	1000	0.12

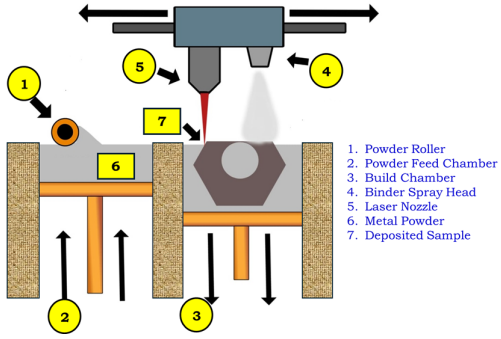

Fig. 1. Schematic of SLM Process

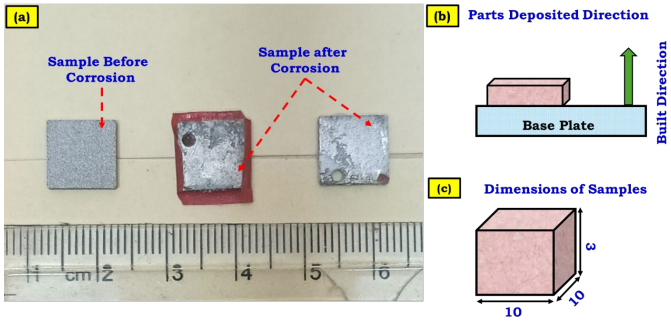

Fig. 2. (a) Samples before and after corrosion (b) Parts deposited direction (c) Sample dimensions

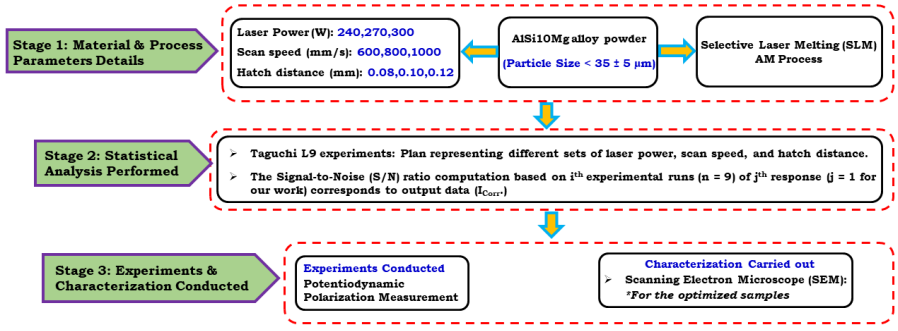

Fig. 3. Flowchart illustrating the SLM process

The experiments to build samples are carried out in an inert environment. The printed sample specimens' dimensions are length x width x height: 10 mm x 10 mm x 10 mm. The cut samples possessing dimensions (length x width x height: 10 mm x 10 mm x 3 mm) were used for corrosion examination. Figure 2 shows samples before and after corrosion, parts deposited direction, and sample dimensions. The flowchart illustrating the methodology used for the present work is shown in Figure 3.

2.2. Experiments and Statistical Analysis

Taguchi L_9 experimental plan representing different sets of laser power, scan speed, and hatch distance is presented in Table 2. Each trial is repeated thrice, and the average values of corrosion behaviour (corrosion current density, i.e., colour) are recorded to perform accurate statistical analysis and optimization.

The signal-to-noise (S/N) ratio computation based on i^{th} experimental runs (n = 9, for the present case) of j^{th} response (j = 1 for our work) corresponds to experimental output data ($I_{Corr.}$), which is presented in Equation 1. S/N ratio is computed correspond to corrosion current density (ICorr.) examined for each experimental run (n = 9).

$$S/N_{lower-the-better} = -10\ \log\left(\frac{1}{n}\sum_{i=1}^{n}\frac{1}{\left(y_{ij}\right)^2}\right) \quad (1)$$

2.3. Preparation of medium and inhibitor

HCl, 99.3% pure, procured from Merck, India, was used to prepare a 1 M HCl solution. 12.5 ml of HCl was dissolved in 500 ml of distilled water, which was initially standardized with NaOH and oxalic acid. The calculated amount of NaCl crystals was dissolved in distilled water to prepare a 0.4 M NaCl solution.

2.4. Potentiodynamic polarization measurement

PDP is an electrochemical technique used to study the corrosion behaviour of materials by measuring their response to an applied potential. This method provides valuable insights into the anodic and cathodic reactions occurring on the material's surface, helping to evaluate inhibitors' corrosion rate, mechanism, and efficacy. The test coupons of dimensions of 1 cm × 1 cm × 0.2 cm) were taken. Before electrochemical studies, the specimen was precisely abraded with 500-1600 SiC papers. The prepared samples were subjected to distilled water washing, flushing, and air drying.

Potentiodynamic polarization studies are conducted on cleaned samples subjected to 1M of solution (HCl) for 30 mins and 0.4 M of NaCl. The sample was first submerged in the corrosive medium for roughly 400 seconds to measure the open-circuit potential (OCP). Experiments were conducted on an electrochemical station CHI660E -CH instrument with a scan rate of 0.1 mVs^{-1}, from −250 mV cathodically to +250 mV anodically. The experimental setup for corrosion rate measurements consists of $AlSi_{10}Mg$ printed sample (working electrode), platinum, anode (counter terminal), and reference cathode (calomel electrode). The Tafel plots data were used to extrapolate the current density (icorr.) obtained viz. anodic and cathodic corrosion potential. All experimental runs are conducted at room temperature. The resulting data points is recorded against the calomel electrode and the corrosion rate was computed from the resulting Tafel graphs.

2.5. Optimization of SLM parameters

The output data (corrosion current) from L9 experiments were transformed to S/N ratio data. The factor analysis is done by estimating the contribution of individual factors on the corrosion current experimental data. The main effect plots are drawn to examine the variable influence when varied between their respective operating levels. The mean values of the S/N ratio at each level for a factor is estimated. The higher value of the S/N ratio corresponds to the levels of each factor determine the optimal condition for the SLM process.

3. Results and Discussion

This section discusses the results of corrosion current influencing variables and optimization of SLM parameters. The model-determined optimal conditions are validated by conducting confirmation experiments and morphological analysis.

3.1. Data collection and Factor analysis

Table 2 shows the input-output data collected according to L_9 Taguchi experiments. The collected data was analyzed for the S/N ratio data corresponding to Icorr. (refer to Table 2).

Table 2.
Input-output data of SLM process

Exp. No.	Input variables			Output Variable			S/N ratio of $I_{Corr.}$ (dB)
	Laser Power, W	Scan Speed, mm/s	Hatch Distance, mm	$i_{corr.}$ (A/cm^2)	$C_R(10^{-4})$ (mpy)	η(%)	
1	240	600	0.08	0.01692	1.844	75.00	95.43
2	240	800	0.10	0.01478	1.611	78.16	96.67
3	240	1000	0.12	0.02170	2.365	67.94	93.27
4	270	600	0.10	0.02084	2.271	69.21	93.62
5	270	800	0.12	0.01651	1.832	75.60	95.65
6	270	1000	0.08	0.01543	1.681	77.20	96.23
7	300	600	0.12	0.01814	1.977	73.20	94.83
8	300	800	0.08	0.03326	3.625	50.86	89.56
9	300	1000	0.10	0.01835	2.000	73.89	94.73

Table 3.
Formulae used to construct Pareto ANOVA for three factor levels

Factors		A	B	C	Total
Sum of factor levels	1	ΣA_1	ΣB_1	ΣC_1	$T = \Sigma A_1 + \Sigma A_2 + \Sigma A_3$
	2	ΣA_2	ΣB_2	ΣC_2	
	3	ΣA_3	ΣB_3	ΣC_3	
Sum of squares of differences		SS_A	SS_B	SS_C	SS_T
Degrees of freedom		2	2	2	8
Percentage contribution ratio		SS_A/SS_T	SS_B/SS_T	SS_C/SS_T	1

$$SS_A = \left(\Sigma A_1 - \Sigma A_2\right)^2 + \left(\Sigma A_1 - \Sigma A_3\right)^2 + \left(\Sigma A_3 - \Sigma A_2\right)^2 ; SS_B = \left(\Sigma B_1 - \Sigma B_2\right)^2 + \left(\Sigma B_1 - \Sigma B_3\right)^2 + \left(\Sigma B_3 - \Sigma B_2\right)^2$$

$$SS_C = \left(\Sigma C_1 - \Sigma C_2\right)^2 + \left(\Sigma C_1 - \Sigma C_3\right)^2 + \left(\Sigma C_3 - \Sigma C_2\right)^2 ; SS_T = SS_A + SS_B + SS_C$$

Table 4.
Results of Pareto ANOVA for Corrosion Current ($I_{Corr.}$)

Factors	Levels	Laser Power	Scan Speed	Hatch Distance	Total
Sum at factor levels	1	285.37*	283.88	281.22	849.99
	2	285.50	281.88	285.02	
	3	279.12	284.23	283.75	
Sum of squares of differences		79.78**	9.65	22.45	111.88
Percent contribution		71.31***	8.62	20.07	100.00
Optimal factor levels		$A_2B_3C_2$ (Not among the L_9 set of experiments)			

285.37* = 95.43 + 96.67 + 93.27 (Laser power variable at Level 1)
79.78** = ((285.37-285.50)^2) + ((285.37-279.12)^2) + ((285.50-279.12)^2)
71.31*** = (100 x 111.88)/79.78

Pareto analysis of the variance table was constructed to estimate the factor effects is presented in Table 3. Pareto analysis of the variance table to estimate the factor effects on Icorr. based on S/N ratio data (refer to Table 4). A higher S/N ratio value ensures better corrosion resistance properties. The main effects at each factor level drawn based on the S/N ratio are presented in Figure 4. Laser power at 240 W (low values) showed lesser corrosion resistance compared to their operating mid-values (270 W). Low laser power might not be sufficient to melt all metal powders because lesser energy density causes weak bonding between powdered particles [23]. The weak bonding ensures the presence of defects (pores, voids, discontinuities, irregularities, etc.) and is treated as activation sites for corrosion [45]. Laser power at a higher (300 W) value resulted in higher energy densities that might often burn out some materials [36]. In general, burnt material possesses lighter densities with many potential defects, which is the driving force to undergo corrosion. Scanning speed at low (600 mm/s) and medium values (800 mm/s) causes melt pool instability. The increase in melt pool surface tension and viscosity causes porosity in metal powders and results in corrosion [46]. Low values of hatch distance (0.08 mm) create an increased area of overlapping scan lines, and low heat input values create gaps due to insufficient fusing of metal powders at high values (0.12 mm) of hatch distance [47, 48]. Therefore, the stable melt pool might achieve mid-values of hatch distance that could result in better mechanical and tribological properties [23]. Higher mechanical properties could result in better corrosion resistance. Higher S/N ratio values corresponding to each factor were determined for their respective operating levels to decide the optimal condition. The optimal conditions (laser power: 270 W; Scan speed: 1000 mm/s; Hatch speed: 0.10 mm) correspond to selective laser melting conditions for offering better corrosion resistance obtained through Pareto ANOVA, which is presented in Table 4. The optimal conditions are found to be different from those of L_9 experiments. This occurred due to the multifactor nature and the optimal conditions thus obtained from the set of $3^3 = 27$ experiments.

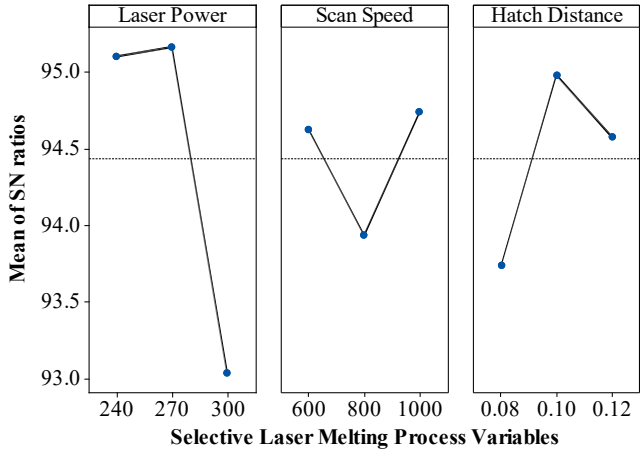

Fig. 4. Main effect plots of SLM variables on corrosion current

3.2. Potentiodynamic studies

The Tafel curves for different selective laser melting condition samples in 1 M HCl acid in the presence and absence of 0.4 M NaCl are given in Figure 5. The potentiodynamic parameters like corrosion current density (Icorr), corrosion rate (CR), and inhibition efficiency (η %) values are reported in Table 2.

From the Tafel plots, the anodic curves represent the metal dissolution process (oxidation), while the cathodic curves correspond to the hydrogen evolution process (reduction). It was observed that the overall shape and characteristics of the plots remained consistent regardless of the presence or absence of an inhibitor. This indicates that the corrosion mechanism of mild steel in 1 M HCl solution remains unchanged in the presence of inhibitors at varying concentrations. A mixed-type inhibition characterized by the corrosion potential (Ecorr) shift that was less than ± 85 mV relative to the Ecorr. of the blank solution. The plot demonstrated its role as a mixed-type inhibitor, suppressing both cathodic and anodic reactions upon adding 0.4 M NaCl. The corrosion rate (CR) and inhibition efficiency (η%) values were calculated using Equations (2) and (3), respectively.

$$\upsilon_{corr}\,(mmy^{-1}) = \frac{k \times i_{corr} \times EW}{\rho} \quad .....(2)$$

$$(IE)\% = \frac{i^{o}_{corr} - i^{i}_{corr}}{i^{o}_{corr}} \quad .....(3)$$

Where, K = 0.00327 mm g/A cm.y^{-1}, icorr. = is the corrosion current density in A/cm^2, ρ = is the density of the material undergoing corrosion, and EW = equivalent weight of the metal.

Here i^{o}_{corr}, and i^{i}_{corr} are the corrosion current density values in the absence and presence of 0.4 M NaCl inhibitor respectively.

Table 2 shows that the corrosion current density (icorr.) and CR increased with the increase in laser power, and there was no substantial change in efficiency with each change in scan rate or laser power.

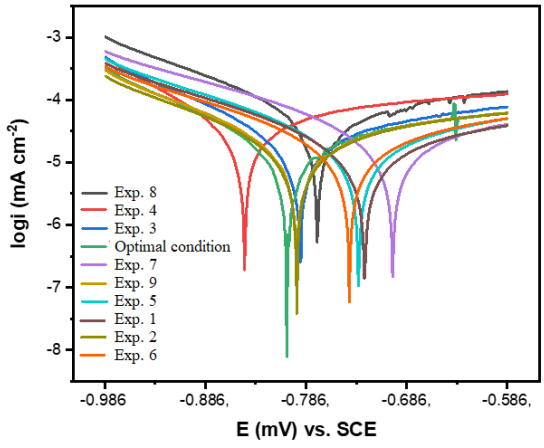

Figure 5. Tafel curves of SLM condition samples.

3.3. Confirmation experiments

Pareto Analysis of variance determined optimal conditions that minimize the corrosion rate are different from those obtained for L$_9$ experiments. Experiments conducted for optimal conditions (laser power: 270 W; Scan speed: 1000 mm/s; Hatch speed: 0.10 mm) resulted in lesser negative values of corrosion potential than that obtained for L$_9$ experiments. The Icorr. value corresponding to optimal condition is 0.00001244 mA/cm^2 (comparatively lesser than those of L$_9$ experiments presented in Table 2). Therefore, Taguchi is one of the cost-effective methods that not only minimizes experiments but also provides detailed process insights (percent contribution of variables and optimal conditions) that improve 16.1% decrease in the response variable (Icorr. value of SLM parts compared with Exp. 2 of Table 2).

3.4. Corrosion morphology samples

Post-corrosion analysis of the microstructure of Corrosion rate of Optimal conditions (Laser power: 270 W; Scan speed: 1000 mm/s; Hatch spacing: 0.10 mm) Shown in Figure 6, and Sub-optimal condition (Laser power: 300 W; Scan speed: 800 mm/s; Hatch spacing: 0.08 mm) shown in Table 2 (experiment 8). Figure 6(a) illustrates the micrograph of AlSi10Mg alloy deposited using the SLM process before corrosion at a magnification of 500x, depicting a reasonably uniform fine-grained surface. Also, a few micrograph areas display duskier spots, which may be due to slight porosity or un-melted particles. Thus, fine textured micrograph signifies a through-melted and relatively homogeneous structure, which is a typical characteristic of the process [13, 24, 49]. The microstructure of the optimal condition, as shown in Figure 6b, at different locations, is observed that the morphology is less corroded with minimum oxidation on the surface. However, in the case of sub-optimal conditions, the surface morphology can be more oxidised, with larger or significant corrosion on the surface at various locations of the sample presented in Figure 6c. The microstructural analysis is clearly in line with the experimental results and Taguchi L_9 analysis and design of experiments. Figure 6 shows the SEM images of metal samples in the absence and presence of 1 M HCl and after adding 0.4M NaCl. Substantial corrosion on the uninhibited metal surface, as indicated by pits and rough surface characteristics, indicates serious surface degradation. The inhibited solution has effectively restricted the corrosion process on the surface treated with 0.4 NaCl, as evidenced by the smoother morphology and less corrosion evidence.

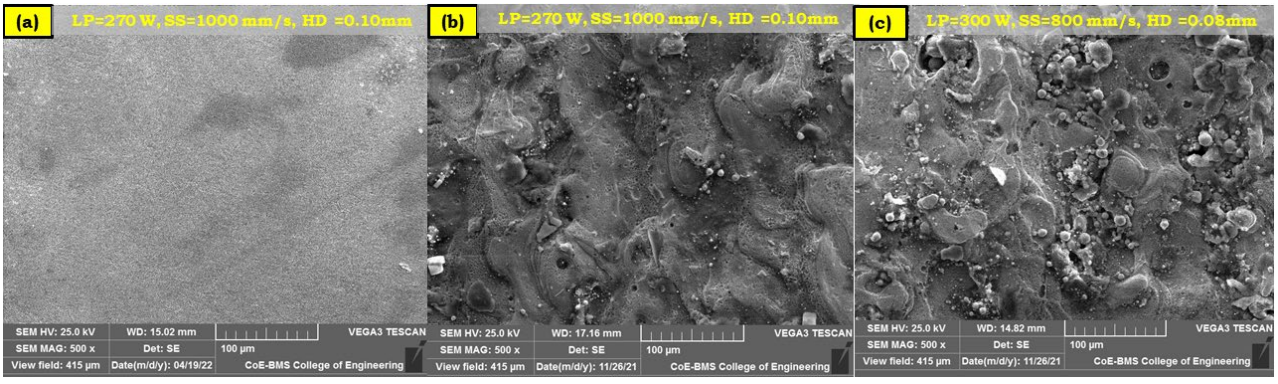

Fig. 6. SEM micrograph of (a) Samples before corrosion (b) Corrosion micrographs at optimal condition (c) Corrosion micrographs at Sub-optimal condition

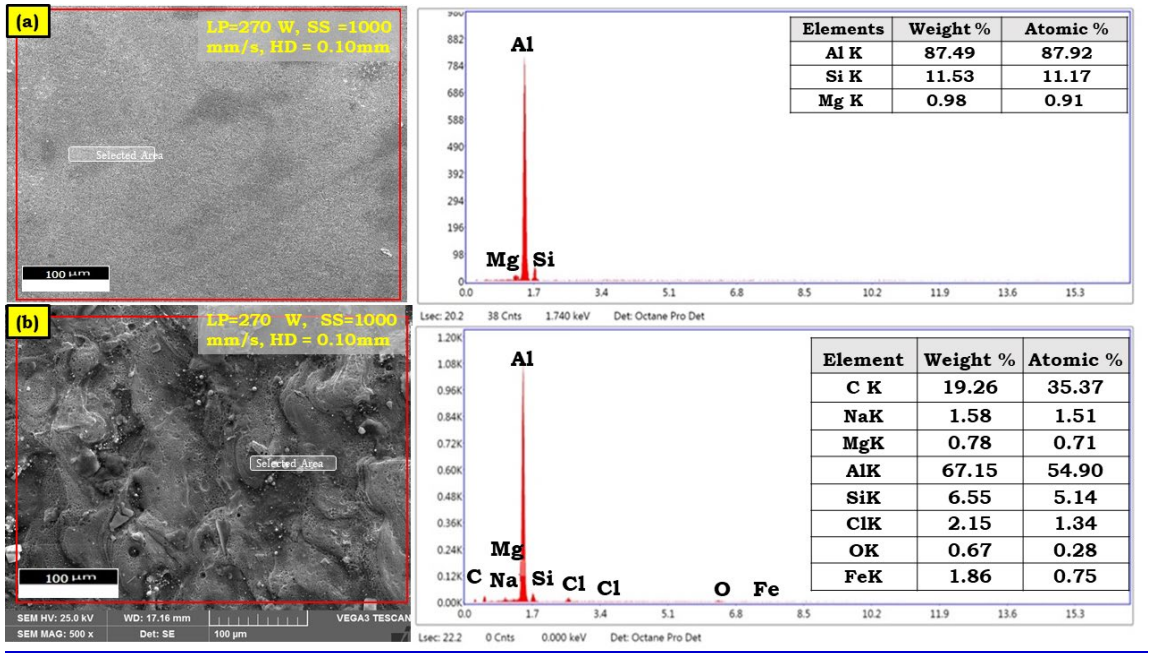

Fig. 7. EDAX analysis of (a) Samples before corrosion (Blank) (b) Corrosion micrographs at Optimal condition

Additionally, corrosion products have been deposited on the uninhabited metal surface, indicating active corrosion. Inhibited surfaces, however, show a significant reduction in these products. Compared to the inhibited sample, the corroded sample shows prominent micro-cracks and fragmented grain boundaries. Figure 7(a) depicts the EDAX analysis of the AlSi10Mg sample (optimal condition) before corrosion, wherein Al is the main element followed by Si and traces of Mg. Figure 7(b) depicts the EDAX analysis of the AlSi10Mg sample (optimal condition) after corrosion, having Al as the main element followed by C, Si, Cl with traces of Na, Fe, Mg and O. Compared to Figure 7(a), the Figure 7(b) display a rugged and uneven face, implying corrosion effects. Carbon and iron content may be due to external contamination or corrosion consequences. Al falls from 87.49% (Figure 7(a)) to 67.15% (Figure 7(a)), which is indicative of material degradation. Also, Na and Cl suggest that the material be exposed to a saline corrosive environment. Overall, the EDAX assessment proves substantial material degradation after corrosion. Na, Cl, and enhanced oxygen imply chloride-induced corrosion activity, which is widespread in environments with saltwater exposure. The loss in Al content and surface roughness further supports the corrosion impact. Analogous interpretations were observed by various researchers [50, 51].

4. Conclusions

The SLM processing route is used to fabricate AlSi10Mg samples useful for corrosive environment applications. Parts that offer better corrosion resistance rely on process variables (LP, SS, and HD). The Taguchi method is used to investigate and optimise process variables to provide better corrosion resistance. The following conclusions are drawn from the present research efforts.

- Taguchi L_9 experiments consist of different sets of conditions (LP, SS, and HD) and are operated at three levels. Pareto analysis of variance ensures that LP contributes 71.31%, HD 20.07%, and SS 8.62% to corrosion current (a way to measure corrosion resistance).
- The optimal conditions (LP: 270 W; SS: 1000 mm/s; HD: 0.10 mm) improved corrosion resistance. These conditions are found to be different from those of the L_9 experiments. This justifies the optimal conditions determined from only nine experimental trials (which reduce material waste, effort, cost, and time) compared to $3^3 = 27$ experiments. Experimental values of corrosion current resulted in 0.00001244 mA/cm^2 (comparatively 16.1% decreased corrosion resistance among the minimum value of L_9 experiments).
- From the SEM morphology, less corrosion with minimum oxidation was observed on the surface with optimal conditions (LP: 270 W; SS: 1000 mm/s; HD: 0.10 mm). However, in the case of Sub-optimal conditions (Experiment 8), more oxidation with more extensive or significant corrosion at various locations was observed on the sample surface

References

[1] Czerwinski, F. (2020). Thermal stability of aluminum alloys. *Materials*. 13(15), 3441, 1-49. https://doi.org/10.3390/ma13153441.

[2] Michi, R.A., Plotkowski, A., Shyam, A., Dehoff, R.R. & Babu, S. S. (2022). Towards high-temperature applications of aluminium alloys enabled by additive manufacturing. *International Materials Reviews.* 67(3), 298-345. https://doi.org/10.1080/09506608.2021.1951580.

[3] Fang, Z., Cao, J., Guan, Y. (2020). *Corrosion control technologies for aluminium alloy vessel*. Springer Singapore.

[4] Davis, J.R. (1999). *Corrosion of aluminium and aluminium alloys*. Asm International.

[5] Ahmed, M.M., El-Sayed Seleman, M.M., Fydrych, D. & Çam, G. (2023). Friction stir welding of aluminium in the aerospace industry: the current progress and state-of-the-art review. *Materials*. 16(8), 2971, 1-33. https://doi.org/10.3390/ma16082971.

[6] Taylor, M.P., Chen, J.J., Young, B.R. (2013). *Control for aluminum production and other processing industries*. CRC Press.

[7] Hadad, M. & Hadi, M. (2013). An investigation on surface grinding of hardened stainless steel S34700 and aluminum alloy AA6061 using minimum quantity of lubrication (MQL) technique. *The International Journal of Advanced Manufacturing Technology*. 68, 2145-2158. https://doi.org/10.1007/s00170-013-4830-3.

[8] Deyab, M.A., Abd El-Rehim, S.S., Hassan, H.H. & Shaltot, A.M. (2020). Impact of rare earth compounds on corrosion of aluminium alloy (AA6061) in the marine water environment. *Journal of Alloys and Compounds*. 820, 153428, 1-7. https://doi.org/10.1016/j.jallcom.2019.153428.

[9] Fathi, P., Rafieazad, M., Duan, X., Mohammadi, M. & Nasiri, A. M. (2019). On microstructure and corrosion behaviour of AlSi10Mg alloy with low surface roughness fabricated by direct metal laser sintering. *Corrosion Science*. 157, 126-145. https://doi.org/10.1016/j.corsci.2019.05.032.

[10] Liao, J., Hotta, M. & Mori, Y. (2012). Improved corrosion resistance of a high-strength Mg–Al–Mn–Ca magnesium alloy made by rapid solidification powder metallurgy. *Materials Science and Engineering: A*, 544, 10-20. https://doi.org/10.1016/j.msea.2012.02.046.

[11] Swamy, P.K., Mylaraiah, S., Gowdru Chandrashekarappa, M.P., Lakshmikanthan, A., Pimenov, D.Y., Giasin, K. & Krishna, M. (2021). Corrosion behaviour of high-strength Al 7005 alloy and its composites reinforced with industrial waste-based fly ash and glass fibre: comparison of stir cast and extrusion conditions. *Materials*. 14(14), 3929, 1-17. https://doi.org/10.3390/ma14143929.

[12] Tofail, S.A., Koumoulos, E.P., Bandyopadhyay, A., Bose, S., O'Donoghue, L. & Charitidis, C. (2018). Additive manufacturing: scientific and technological challenges, market uptake and opportunities. *Materials Today*. 21(1), 22-37. https://doi.org/10.1016/j.mattod.2017.07.001.

[13] Gadlegaonkar, N., Bansod, P.J., Lakshmikanthan, A. & Bhole, K. (2025). A Review on additively manufactured

AlSi10Mg alloy: mechanical, tribological, and microstructure properties. *Journal of Mines, Metals and Fuels*. 87-101.

[14] Wang, C., Tan, X.P., Tor, S.B. & Lim, C.S. (2020). Machine learning in additive manufacturing: State-of-the-art and perspectives. *Additive Manufacturing*. 36, 101538, 1-20. https://doi.org/10.1016/j.addma.2020.101538.

[15] Pelevin, I.A., Nalivaiko, A.Y., Ozherelkov, D.Y., Shinkaryov, A.S., Chernyshikhin, S.V., Arnautov, A.N., Zmanovsky, S.V. & Gromov, A.A. (2021). Selective laser melting of Al-based matrix composites with Al2O3 reinforcement: Features and advantages. *Materials*. 14(10), 2648, 1-17. https://doi.org/10.3390/ma14102648.

[16] Fang, Z.C., Wu, Z.L., Huang, C.G. & Wu, C.W. (2020). Review on residual stress in selective laser melting additive manufacturing of alloy parts. *Optics & Laser Technology*. 129, 106283, 1-15. https://doi.org/10.1016/j.optlastec.2020.106283.

[17] Ren, S., Chen, Y., Liu, T., & Qu, X. (2019). Effect of build orientation on mechanical properties and microstructure of Ti-6Al-4V manufactured by selective laser melting. *Metallurgical and Materials Transactions A*. 50(9), 4388-4409. https://doi.org/10.1007/s11661-019-05322-w.

[18] Li, C., Liu, J.F., Fang, X.Y. & Guo, Y.B. (2017). Efficient predictive model of part distortion and residual stress in selective laser melting. *Additive Manufacturing*. 17, 157-168. https://doi.org/10.1016/j.addma.2017.08.014.

[19] Zhao, L., Macías, J.G.S., Dolimont, A., Simar, A. & Rivière-Lorphèvre, E. (2020). Comparison of residual stresses obtained by the crack compliance method for parts produced by different metal additive manufacturing techniques and after friction stir processing. *Additive Manufacturing*. 36, 101499, 1-13. https://doi.org/10.1016/j.addma.2020.101499.

[20] Lou, X., Othon, M.A. & Rebak, R.B. (2017). Corrosion fatigue crack growth of laser additively-manufactured 316L stainless steel in high temperature water. *Corrosion science*. 127, 120-130. https://doi.org/10.1016/j.corsci.2017.08.023.

[21] Kong, D., Dong, C., Ni, X. & Li, X. (2019). Corrosion of metallic materials fabricated by selective laser melting. *Materials Degradation*. 3(1), 1-14. https://doi.org/10.1038/s41529-019-0086-1.

[22] Jeyaprakash, N., Yang, C.H., Karuppasamy, S.S. & Rajendran, D.K. (2022). Correlation of microstructural with corrosion behaviour of Ti-6Al-4V specimens developed through selective laser melting technique. *Proceedings of the Institution of Mechanical Engineers, Part E: Journal of Process Mechanical Engineering*. 236(5), 2240-2251. https://doi.org/10.1177/09544089221087823.

[23] Rohith, S., Mohan, N., Malik, V., Saxena, K.K. & Prasad, M.A. (2023). Modelling and optimization of selective laser melting parameters using Taguchi and super ranking concept approaches. *International Journal on Interactive Design and Manufacturing*. (IJIDeM). 17(5), 2415-2427. https://doi.org/10.1007/s12008-022-01011-y.

[24] Sheshadri, R., Nagaraj, M., Lakshmikanthan, A., Chandrashekarappa, M.P.G., Pimenov, D.Y., Giasin, K., Prasad, R.V.S. & Wojciechowski, S. (2021). Experimental investigation of selective laser melting parameters for higher surface quality and microhardness properties: taguchi and super ranking concept approaches. *Journal of Materials Research and Technology*. 14, 2586-2600. https://doi.org/10.1016/j.jmrt.2021.07.144.

[25] Romano, J., Ladani, L. & Sadowski, M. (2016). Laser additive melting and solidification of Inconel 718: Finite element simulation and experiment. *The Journal of The Minerals, Metals & Materials Society (TMS)*. 68(3), 967-977. https://doi.org/10.1007/s11837-015-1765-1.

[26] Yang, Y., Knol, M.F., Van Keulen, F. & Ayas, C. (2018). A semi-analytical thermal modelling approach for selective laser melting. *Additive Manufacturing*. 21, 284-297. https://doi.org/10.1016/j.addma.2018.03.002.

[27] Ansari, M.J., Nguyen, D.S. & Park, H.S. (2019). Investigation of SLM process in terms of temperature distribution and melting pool size: Modeling and experimental approaches. *Materials*. 12(8), 1272, 1-18. https://doi.org/10.3390/ma12081272.

[28] Dong, Z., Liu, Y., Wen, W., Ge, J. & Liang, J. (2018). Effect of hatch spacing on melt pool and as-built quality during selective laser melting of stainless steel: Modeling and experimental approaches. *Materials*. 12(1), 50, 1-15. https://doi.org/10.3390/ma12010050.

[29] Wang, X., Lu, Q., Zhang, P., Yan, H., Shi, H., Sun, T., Zhou, K. & Chen, K. (2024). A review on the simulation of selective laser melting AlSi10Mg. *Optics & Laser Technology*. 174, 110500, 1-32. https://doi.org/10.1016/j.optlastec.2023.110500.

[30] Razavykia, A., Brusa, E., Delprete, C. & Yavari, R. (2020). An overview of additive manufacturing technologies—a review to technical synthesis in numerical study of selective laser melting. *Materials*. 13(17), 3895, 1-22. https://doi.org/10.3390/ma13173895.

[31] Korkmaz, M.E., Gupta, M.K., Robak, G., Moj, K., Krolczyk, G.M. & Kuntoğlu, M. (2022). Development of lattice structure with selective laser melting process: A state of the art on properties, future trends, and challenges. *Journal of Manufacturing Processes*. 81, 1040-1063. https://doi.org/10.1016/j.jmapro.2022.07.051.

[32] Gunasekaran, J., Sevvel, P. & Solomon, I.J. (2021). Metallic materials fabrication by selective laser melting: A review. *Materials Today: Proceedings*. 37, 252-256. https://doi.org/10.1016/j.matpr.2020.05.162.

[33] Jiang, H.Z., Li, Z.Y., Feng, T., Wu, P.Y., Chen, Q.S., Feng, Y.L., Li, S.W., Gao, H. & Xu, H.J. (2019). Factor analysis of selective laser melting process parameters with normalised quantities and Taguchi method. *Optics & Laser Technology*. 119, 105592, 1-11. https://doi.org/10.1016/j.optlastec.2019.105592.

[34] Amir, B., Gale, Y., Sadot, A., Samuha, S. & Sadot, O. (2022). Study on the effects of manufacturing parameters on the dynamic properties of AlSi10Mg under dynamic loads using Taguchi procedure. *Materials & Design*. 111125, 1-11. https://doi.org/10.1016/j.matdes.2022.111125.

[35] Khorasani, A., Gibson, I., Awan, U.S. & Ghaderi, A. (2019). The effect of SLM process parameters on density, hardness, tensile strength, and surface quality of Ti-6Al-4V. *Additive manufacturing*. 25, 176-186. https://doi.org/10.1016/j.addma.2018.09.002.

[36] Olakanmi, E.O., Cochrane, R.F. & Dalgarno, K.W. (2015). A review on selective laser sintering/melting (SLS/SLM) of aluminium alloy powders: Processing, microstructure, and properties. *Progress in materials science*. 74, 401-477. https://doi.org/10.1016/j.pmatsci.2015.03.002.

[37] Trevisan, F., Calignano, F., Lorusso, M., Pakkanen, J., Aversa, A., Ambrosio, E.P., Lombardi, M., Fino, P. & Manfredi, D. (2017). On the selective laser melting (SLM) of the AlSi10Mg alloy: process, microstructure, and mechanical properties. *Materials.* 10(1), 76, 1-23. https://doi.org/10.3390/ma10010076.

[38] Li, Y. & Gu, D. (2014). Parametric analysis of thermal behavior during selective laser melting additive manufacturing of aluminum alloy powder. *Materials & design*. 63, 856-867. https://doi.org/10.1016/j.matdes.2014.07.006.

[39] Aboulkhair, N.T., Simonelli, M., Parry, L., Ashcroft, I., Tuck, C. & Hague, R. (2019). 3D printing of Aluminium alloys: Additive Manufacturing of Aluminium alloys using selective laser melting. *Progress in materials science.* 106, 100578, 1-45. https://doi.org/10.1016/j.pmatsci.2019.100578.

[40] Gu, D., Shi, Q., Lin, K. & Xi, L. (2018). Microstructure and performance evolution and underlying thermal mechanisms of Ni-based parts fabricated by selective laser melting. *Additive Manufacturing*. 22, 265-278. https://doi.org/10.1016/j.addma.2018.05.019.

[41] Read, N., Wang, W., Essa, K. & Attallah, M.M. (2015). Selective laser melting of AlSi10Mg alloy: Process optimisation and mechanical properties development. *Materials & Design (1980-2015)*. 65, 417-424. https://doi.org/10.1016/j.matdes.2014.09.044.

[42] Aboulkhair, N.T., Everitt, N.M., Ashcroft, I. & Tuck, C. (2014). Reducing porosity in AlSi10Mg parts processed by selective laser melting. *Additive manufacturing.* 1-4, 77-86. https://doi.org/10.1016/j.addma.2014.08.001.

[43] Sun, D., Gu, D., Lin, K., Ma, J., Chen, W., Huang, J., Sun, X. & Chu, M. (2019). Selective laser melting of titanium parts: Influence of laser process parameters on macro-and microstructures and tensile property. *Powder Technology*. 342, 371-379. https://doi.org/10.1016/j.powtec.2018.09.090.

[44] Majeed, A., Ahmed, A., Salam, A. & Sheikh, M.Z. (2019). Surface quality improvement by parameters analysis, optimization and heat treatment of AlSi10Mg parts manufactured by SLM additive manufacturing. *International Journal of Lightweight Materials and Manufacture.* 2(4), 288-295. https://doi.org/10.1016/j.ijlmm.2019.08.001.

[45] Wang, Z., Ummethala, R., Singh, N., Tang, S., Suryanarayana, C., Eckert, J. & Prashanth, K.G. (2020). Selective laser melting of aluminum and its alloys. *Materials*. 13(20), 4564, 1-68. https://doi.org/10.3390/ma13204564.

[46] Pal, S., Lojen, G., Hudak, R., Rajtukova, V., Brajlih, T., Kokol, V. & Drstvenšek, I. (2020). As-fabricated surface morphologies of Ti-6Al-4V samples fabricated by different laser processing parameters in selective laser melting. *Additive Manufacturing*. 33, 101147, 1-14. https://doi.org/10.1016/j.addma.2020.101147.

[47] Tian, Y., Tomus, D., Rometsch, P. & Wu, X. (2017). Influences of processing parameters on surface roughness of Hastelloy X produced by selective laser melting. *Additive Manufacturing*. 13, 103-112. https://doi.org/10.1016/j.addma.2016.10.010.

[48] Xia, M., Gu, D., Yu, G., Dai, D., Chen, H. & Shi, Q. (2016). Influence of hatch spacing on heat and mass transfer, thermodynamics, and laser processability during additive manufacturing of Inconel 718 alloy. *International Journal of Machine Tools and Manufacture*. 109, 147-157. https://doi.org/10.1016/j.ijmachtools.2016.07.010.

[49] Sahadevan, P., Chithirai, P.S., Lakshmikanthan, A., Bhaumik, A. & Cuautle, A.F. (2024). Effect of printing process parameters on tensile strength and wear rate of 17-4PH stainless steel deposited using SLM process. *Frattura Integrita Strutt*. 18(70), 157-176. https://doi.org/10.3221/IGF-ESIS.70.09 .

[50] Garcia-Cabezon, C., Castro-Sastre, M.A., Fernandez-Abia, A.I., Rodriguez-Mendez, M.L. & Martin-Pedrosa, F. (2022). Microstructure–hardness–corrosion performance of 17–4 precipitation hardening stainless steels processed by selective laser melting in comparison with commercial alloy. *Metals and Materials International.* 28, 2652-2667. https://doi.org/10.1007/s12540-021-01155-8.

[51] Sahadevan, P., Pon Selvan, C., Manjunath Patel, G.C. & Bhaumik, A. (2023). Selective laser melting process parameter optimization on density and corrosion resistance of 17-4PH stainless steel. *Archives of Foundry Engineering.* 23(4), 105-116. DOI: 10.24425/afe.2023.146685.